Supporting Information

Layered Indium-Silver-Based Hybrid Perovskite Single Crystals for High-Performance X-ray Detection

Luying Zheng,[a,b,d] Binyan Qiu,[a,b] Xin Huang,[b] Yi Zheng,[b] Min Chen,[b] Xiaoming Jiang,[b] Xieming Xu,*[b, c] Shaofan Wu,[b] and Shuaihua Wang*[b, c]

a. College of Chemistry and Materials Science, Fujian Normal University, Fuzhou, 350117, PR China.

b. Key Laboratory of Optoelectronic Materials Chemistry and Physics, Fujian Institute of Research on the Structure of Matter, Chinese Academy of Sciences, Fuzhou, 350002, China.

c. Fujian Science & Technology Innovation Laboratory for Optoelectronic Information of China, Fuzhou, Fujian 350108, China.

d. Fujian College, University of Chinese Academy of Sciences, Fuzhou, Fujian 350002, China

E-mail: shwang@fjirsm.ac.cn.

Experimental Section

Materials

1,4-Butanediamine Dihydrobromide ($BDABr_2$; > 99.9%), bromargyrite (AgBr; > 99.9%), Indium bromide ($InBr_3$; > 99.9%), hydrobromic acid (HBr; 48% aqueous solution), were purchased from Aladdin. We confirm that all reagents and chemicals were used as received without further purification.

Crystal growth

$BDA_2AgInBr_8$: Add 0.16 g MABr and 0.518 g $SnBr_2$ to the PTFE-lined reactor vessel. Then add 3.5 mL hydrobromic acid and 0.5 mL hypophosphorous acid. Place in a 100°C forced air drying oven, maintain for 4 hours, then cool to 80°C at a rate of 1°C/h, followed by cooling to 30°C at a rate of 0.2°C/h.

Material Property Characterization

Power X-ray diffraction patterns were obtained on a Rigaku Miniflex600 diffractometer using Cu Kα radiation (40 kV, 15 mA) with a step size of 0.02°. Crystal structure and orientation were determined on a Synergy Custom (Liquid MetalJet D2+). UV-visible absorption spectra in the 390-800 nm range were obtained using a Hitachi U4100UV spectrophotometer. Thermogravimetric analysis was performed on a Setaram Setsys16 thermogravimetric analyzer under a continuous nitrogen flow.

X-ray detection

A tungsten anode X-ray tube with 50 kV voltage (Moxtek TUB00154-W06) was used to provide a continuous X-ray, and a self-built chopper manufactured by lead sheets of 0.5 mm was used to produce a pulsed X-ray beam. A dosimeter (Radical AGDM+) with a Radical 10X6-180 ion chamber was used to calibrate X-ray dose rates, and 2 mm and 10 mm Aluminum plates as attenuators were employed to achieve a low dose rate. To provide the bias voltage and record current data, a computer-controlled source meter (Keithley Model 2450) with a test fixture (Keithley Model 8101-PIV) was employed. All X-ray experiments were performed in a dark, closed room (40-50 % relative humidity) that was controlled from outside the room by the researcher.

First-principles calculation

The density functional theory calculations were performed using the Vienna ab initio simulation package (VASP), including the effect of core electrons, were described using the projector augmented wave method. Perdew–Burke–Ernzerhf, generalized gradient approximation, and exchange-correlation functionals were used to relax the structural configurations and calculate the band structure. A plane-wave energy cutoff of 520 eV and a k-point mesh of 3×3×3 was used in the electronic self-consistency. All structures were geometrically relaxed until the total force on each ion was below 0.01 eV $Å^{-1}$. The K-points were defined as follows: Γ (0 0 0), X (0.5 0 0), Y (0 0.5 0), Z (0 0 0.5), R_2 (−0.5 −0.5 0.5), R_2 (−0.5 −0.5 0.5), T_2 (0 −0.5 0.5), U_2 (−0.5 0 0.5), V_2 (0.5 −0.5 0).

Figure Section

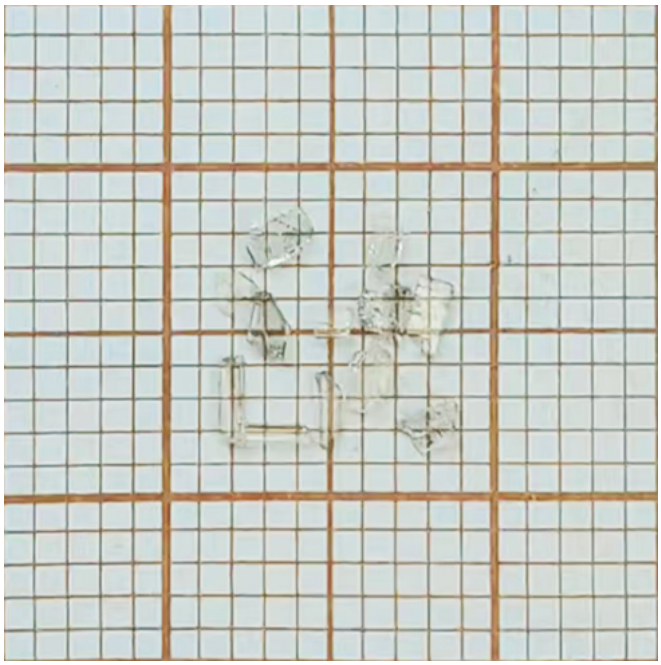

Figure S1. Photograph of $BDA_2AgInBr_8$ crystal.

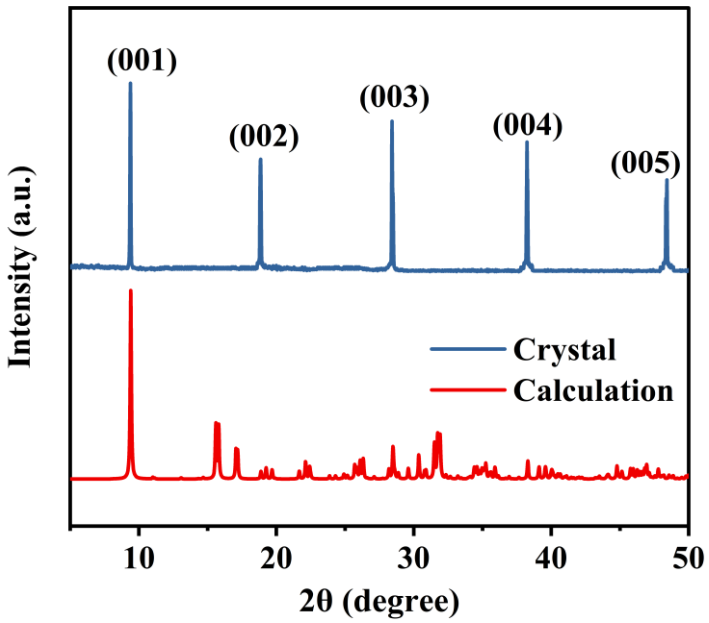

Figure S2. Single-crystal X-ray diffraction pattern of $BDA_2AgInBr_8$.

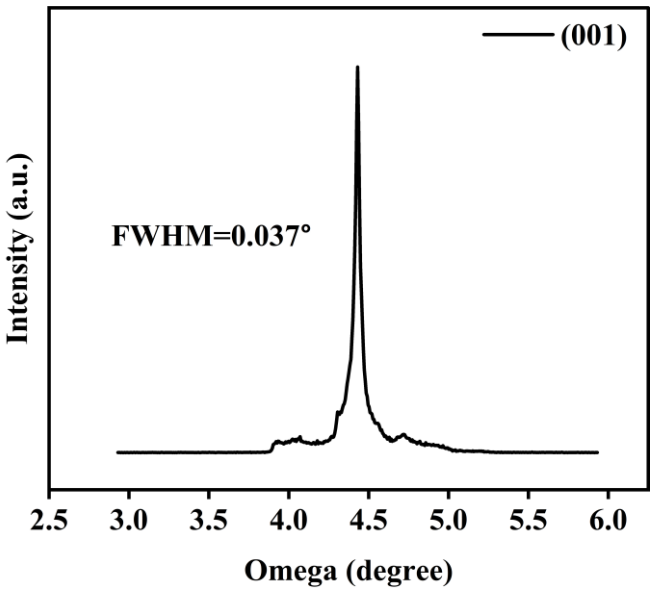

Figure S3. Rocking curve of the (001) diffraction peak for the $BDA_2AgInBr_8$ single crystal.

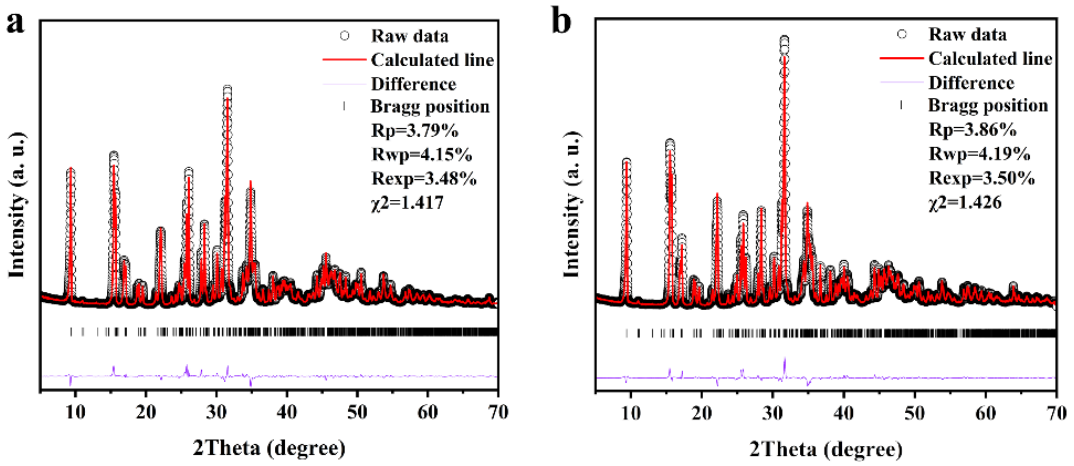

Figure S4. Rietveld refinement of powder XRD patterns for (a) freshly ground $BDA_2AgInBr_8$ sample and (b) sample stored at 80% relative humidity for 36 days.

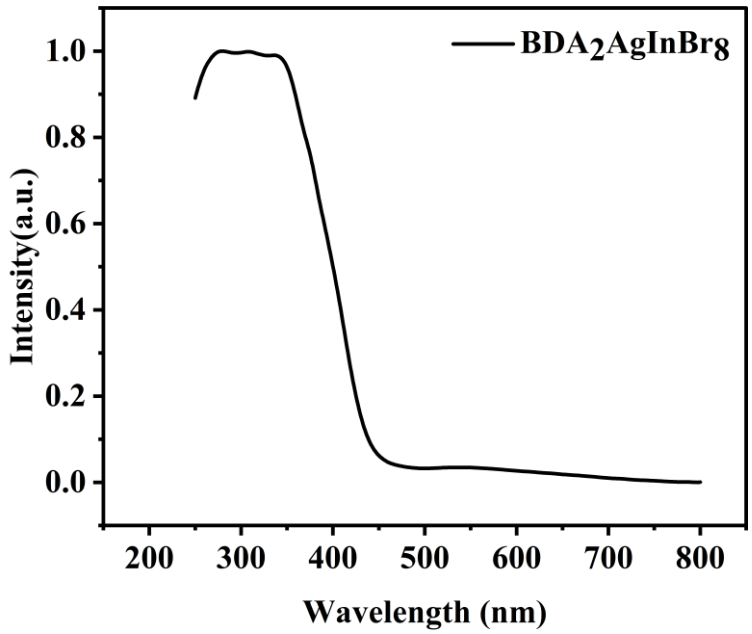

Figure S5. Ultraviolet absorption spectrum of $BDA_2AgInBr_8$ crystals.

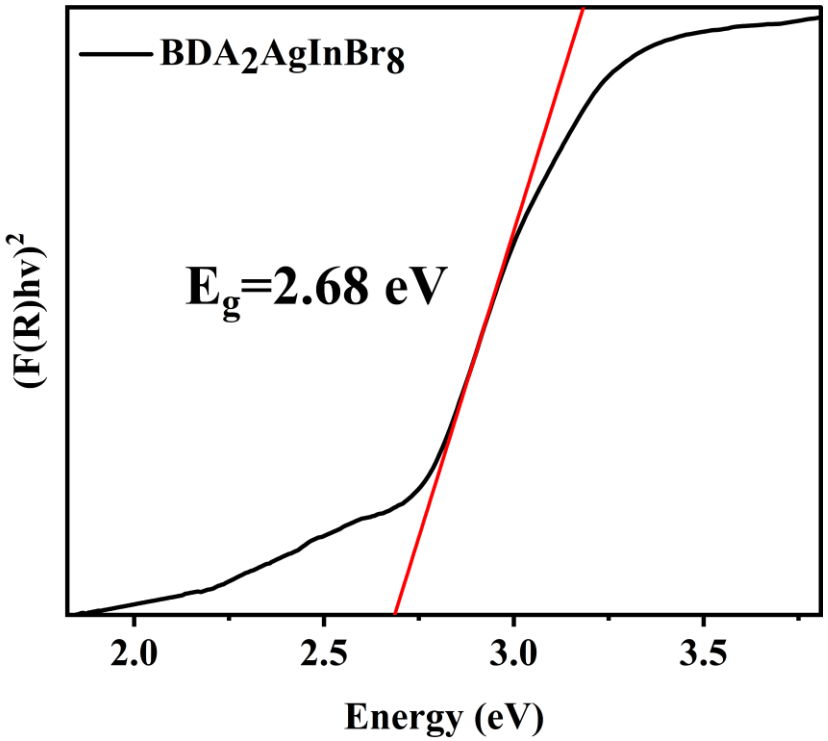

Figure S6. Optical bandgap of $BDA_2AgInBr_8$ crystals.

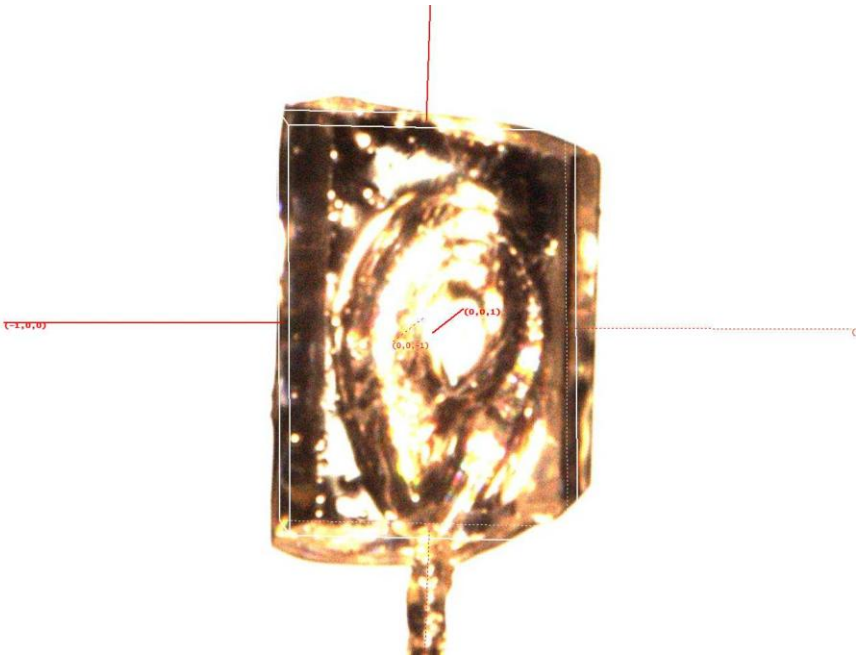

Figure S7. Photographic image of the orientation of $BDA_2AgInBr_8$ single crystals.

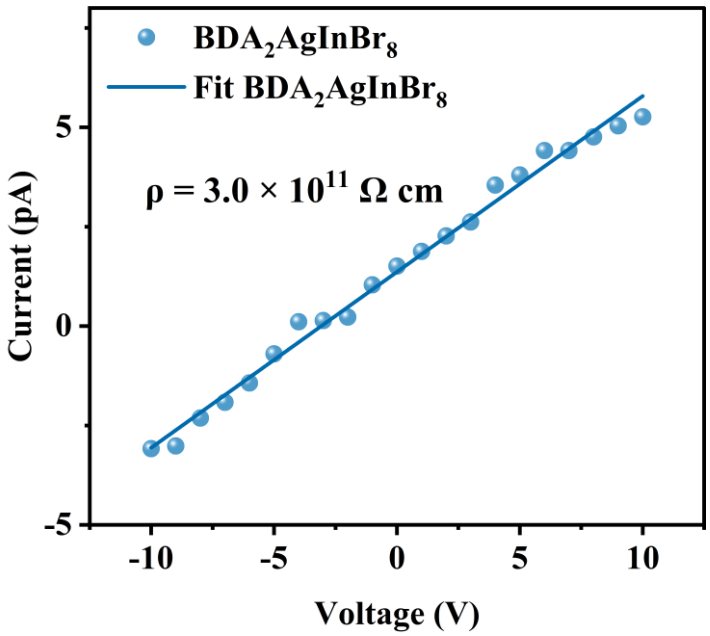

Figure S8. Resistivity of $BDA_2AgInBr_8$.

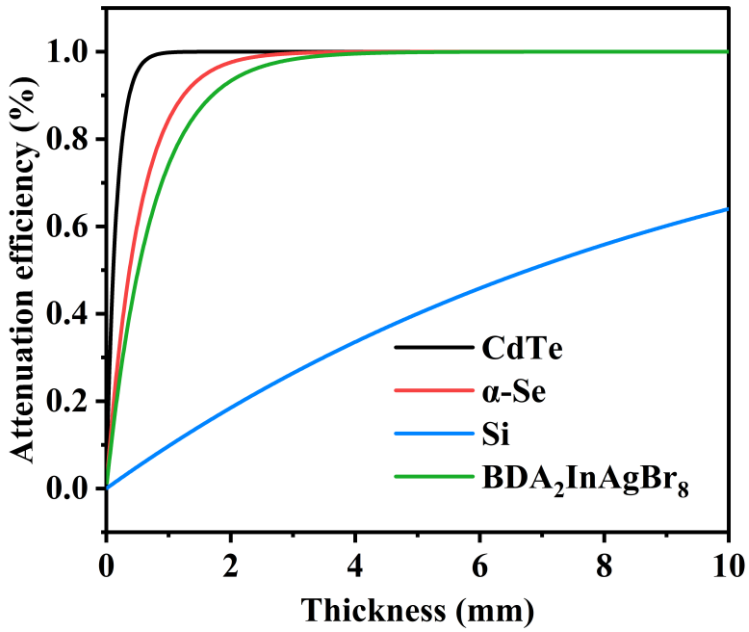

Figure S9. Attenuation efficiency of $BDA_2AgInBr_8$ at 50 keV.

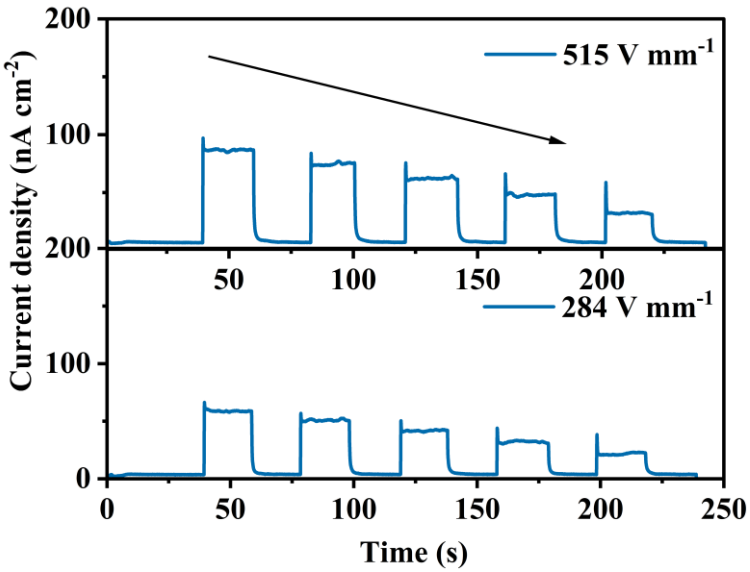

Figure S10. Photocurrent density of $BDA_2AgInBr_8$ under different dose rates.

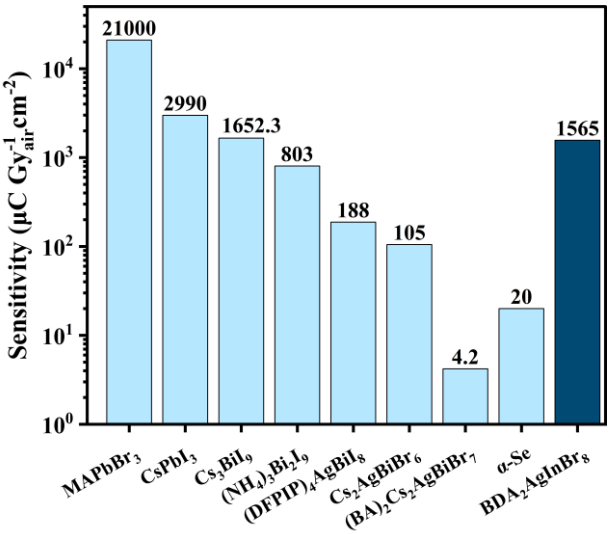

Figure S11. The comparison of sensitivity among commercial scintillation semiconductors, lead-based perovskites, and lead-free perovskites.

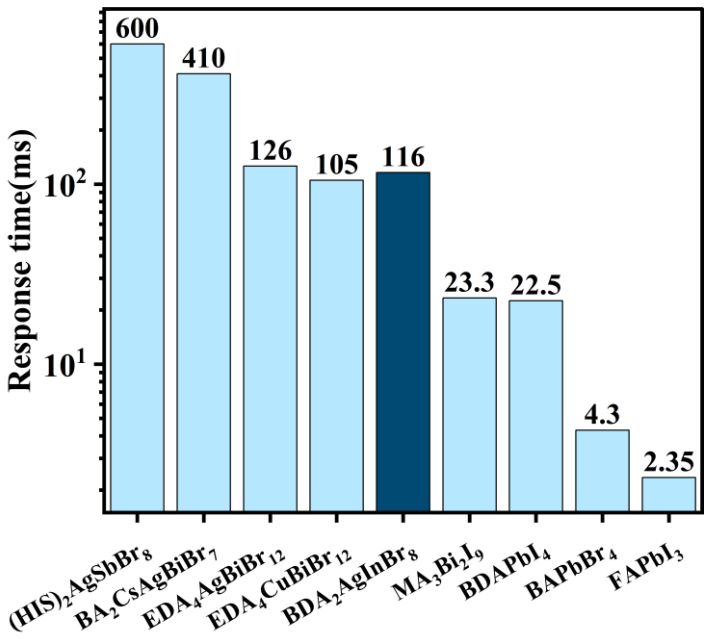

Figure S12. Response time comparison of $BDA_2AgInBr_8$ with other lead-free perovskites and representative lead-based perovskites.

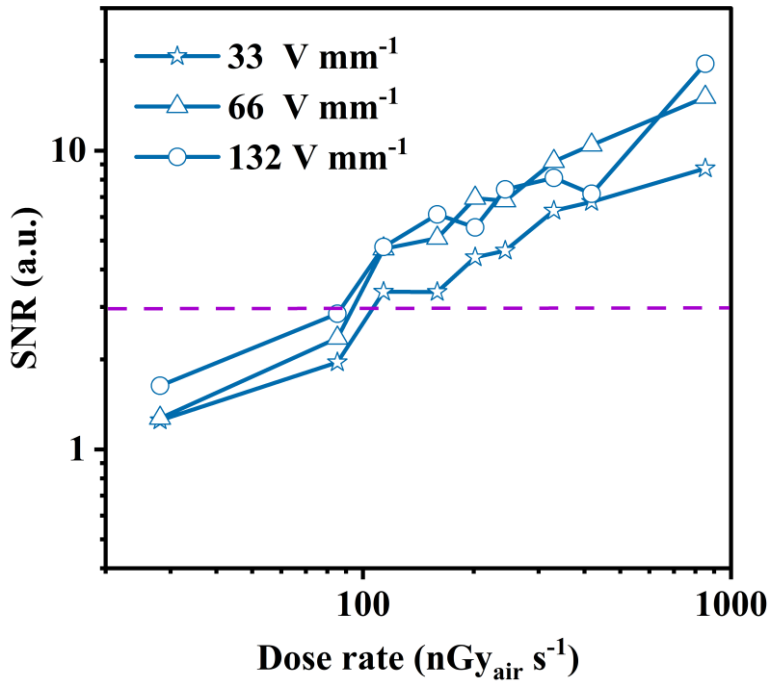

Figure S13. Signal-to-noise ratio (SNR) of $BDA_2AgInBr_8$ under different dose rates and electric field strengths.

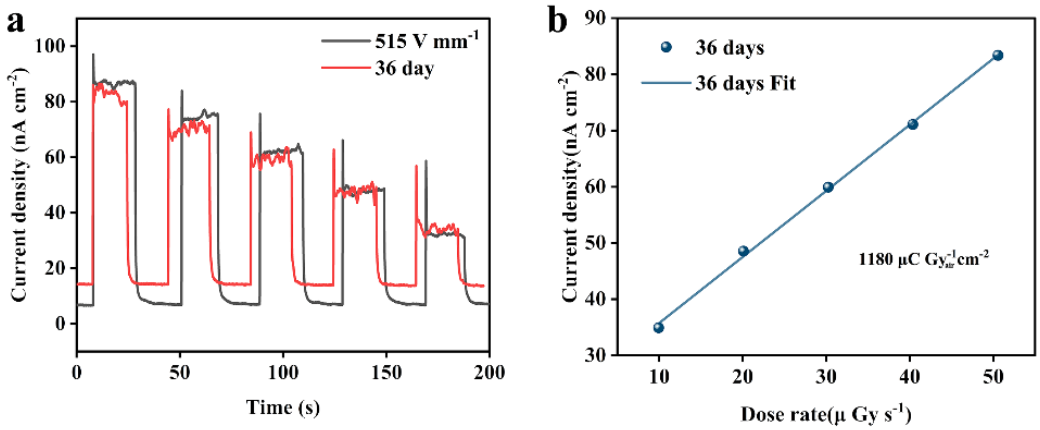

Figure S14. X-ray detection performance of detector after storage at 25 °C and 60% relative humidity for 36 days. (a) Time-dependent current density response under intermittent X-ray irradiation at an electric field of 515 V mm^{-1}. (b) Linear fit of current density versus X-ray dose rate.

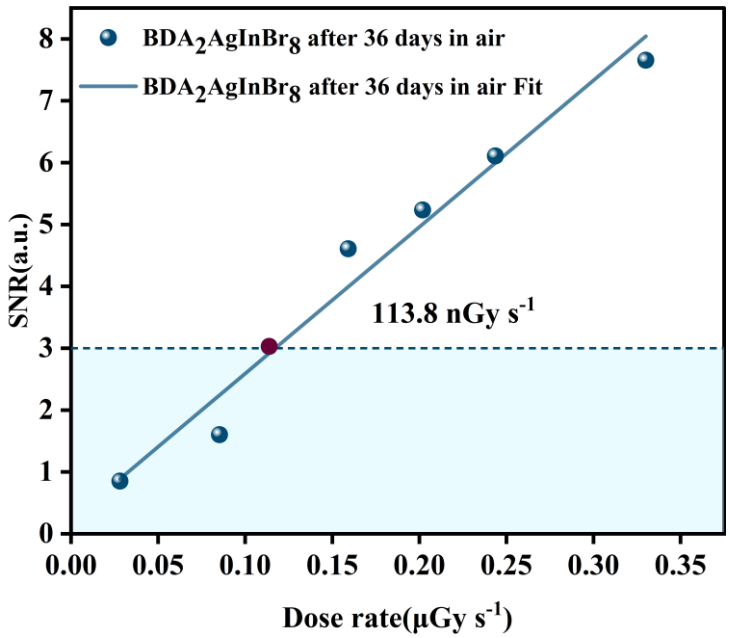

Figure S15. Signal-to-noise ratio of $BDA_2AgInBr_8$ under different dose rates after 36 days of exposure at 25 °C and 60% relative humidity.

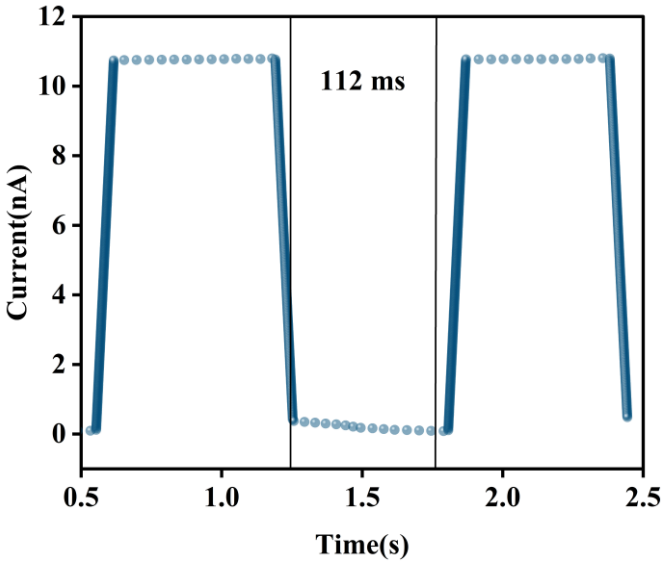

Figure S16. Time-resolved photocurrent response of $BDA_2AgInBr_8$ after 36 days of exposure at 25 °C and 60% relative humidity.

Table Section

Table S1. Crystal data of $BDA_2AgInBr_8$.

Compound	**$BDA_2AgInBr_8$**
Empirical	$(NH_3(CH_2)_4NH_3)_2AgInBr_8$
Formula weight	1042.31
Crystal system	Triclinic
Space group	$P\bar{1}$
a (Å)	8.03130(10)
b(Å)	8.08910(10)
c (Å)	9.59210(10)
α (deg)	101.6290(10)
β (deg)	91.2930(10)
γ (deg)	90.4610(10)
V ($Å^3$)	610.163(12)
Z	1
ρ (calcd) (g/cm^3)	2.837
μ (mm^{-1})	20.001
GOF on F^2	1.062
R_1/wR_2[Fo 2 >2σ(Fo^2)][a]	0.0181/0.0443
R_1/wR_2 (all data)	0.0187/0.0446

$R_1(F)=\sum||F_o| - |F_c||/\sum|F_o|$; $wR_2(F_o^2)=[\sum w(F_o^2 - F_c^2)^2/\sum w(F_o^2)^2]^{1/2}$

Table S2. Electronic band structure with or without spin-orbit coupling effect (SOC)

Compound		**without SOC**			**With SOC**	
	Band gap value	**VBM**	**CBM**	**Band gap value**	**VBM**	**CBM**
$BDA_2AgInBr_8$	1.8205	R_2	X	1.8158	R_2	X

Table S3. Crystal data of $BDA_2AgInBr_8$.

Materials	Sensitivity ($\mu CGy^{-1}cm^{-2}$)	Detection Limits (μGys^{-1})	rise time (ms)	fall time (ms)
$(BA)_2PbI_4$ SC [1]	148	0.241	4.5	4.3
BA_2PbBr_4 SC [2]	726.18	0.0082	3.2	3.5
PEA_2PbBr_4 film [3]	806	0.042	0.147±0.010	0.768±0.109
$(F\text{-}PEA)_2PbI_4$ SC [4]	3402	0.023	–	–
$BA_2EA_2Pb_3Br_{10}$ SC[5]	6800	5.5	–	–
$(BA)_2(MA)_2Pb_3I_{10}$ film[6]	2.76×10^5	10	<0.0005	0.02-0.06
$(C_4H_9NH_3)_2PbBr_4$ SC [7]	236	22.7	–	<100
$BDA_2AgInBr_8$ SC (our work)	1565	120		116

Reference

[1] J. Yukta Ghosh, M. A. Afroz, S. Alghamdi, P. J. Sellin and S. Satapathi, *ACS Photonics* 2022, **9**, 3529–3539.

[2] X. Xu, Y. Wu, Y. Zhang, X. Li, F. Wang, X. Jiang and S. Wang, *Energy Environ. Mater*. 2024, **7**, e12487.

[3] F. Lédée, A. Ciavatti, M. Verdi, L. Basiricò and B. Fraboni, *Adv. Opt. Mater*. 2022, **10**, 2101145.

[4] H. Li, J. Song, W. Pan, D. Xu, W. A. Zhu, H. Wei and B. Yang, *Adv. Mater*. 2020, **32**, 2003790.

[5] C. Ji, S. Wang, Y. Wang, H. Chen, L. Li, Z. Sun and J. Luo, Adv. *Funct. Mater*. 2020, **30**, 1905529.

[6] H. Tsai, F. Liu, S. Shrestha, K. Fernando, S. Tretiak, B. Scott and W. Nie, *Sci. Adv*. 2020, **6**, eaay0815.

[7] Y. Chen, Y. Sun, J. Peng, J. Tang, K. Zheng and Z. Liang, *Adv. Mater*. 2018, **30**, 1703487.